International Journal of Nanomedicine

Dovepress
open access to scientific and medical research

Open Access Full Text Article

ORIGINAL RESEARCH

Tumour-Targeted and Redox-Responsive Mesoporous Silica Nanoparticles for Controlled Release of Doxorubicin and an siRNA Against Metastatic Breast Cancer

This article was published in the following Dove Press journal:
International Journal of Nanomedicine

Jialang Zhuang[1,2,*]
Siqi Chen[1,3,*]
Ye Hu[1]
Fan Yang[1]
Qin Huo[1]
Ni Xie[1]

[1]Biobank, Shenzhen Second People's Hospital, First Affiliated Hospital of Shenzhen University, Shenzhen, 518035, People's Republic of China; [2]Shenzhen Institute of Advanced Technology, Chinese Academy of Sciences, Shenzhen, 518035, People's Republic of China; [3]Graduate School of Guangzhou Medical University, Guangzhou, 510182, People's Republic of China

*These authors contributed equally to this work

Introduction: Metastatic breast cancer seriously harms women's health and is currently the tumour type with the highest mortality rate in women. Recently, the combinatorial therapeutic approaches that integrate anti-cancer drugs and genetic agents is an attractive and promising strategy for the treatment of metastatic breast cancer. Moreover, such a combination strategy requires better drug carriers that can effectively deliver the cargo to the breast cancer cells and achieve controlled release in the cells to achieve better therapeutic effects.

Methods: The tumour-targeted and redox-responsive mesoporous silica nanoparticles (MSNs) functionalised with DNA aptamers (AS1411) as a co-delivery system was developed and investigated for their potential against metastatic breast cancer. Doxorubicin (Dox) was loaded onto the MSNs, while AS1411 and a small interfering RNA (siTIE2) were employed as gatekeepers via attachment to the MSNs with redox-sensitive disulfide bonds.

Results: The controlled release of Dox and siTIE2 was associated with intracellular glutathione. AS1411 mediated the targeted delivery of Dox by increasing its cellular uptake in metastatic breast cancer, ultimately resulting in a lower IC50 in MDA-MB-231 cells (human breast cancer cell line with high metastatic potency), improved biodistribution in tumour-bearing mice, and enhanced in vivo anti-tumour effects. The in vitro cell migration/invasion assay and in vivo anti-metastatic study revealed synergism in the co-delivery system that suppresses cancer cell metastasis.

Conclusion: The tumour-targeted and redox-responsive MSN prepared in this study are promising for the effective delivery and controlled release of Dox and siTIE2 for improved treatment of metastatic breast cancer.

Keywords: drug delivery, mesoporous silica nanoparticles, DNA aptamer, controlled release, metastatic breast cancer

Introduction

Metastatic breast cancer accounts for a majority of deaths from breast cancer worldwide.[1] Whether metastatic breast cancer is the first diagnosis or a recurrence after treatment for early-stage breast cancer, it is rarely curable. Extensive evidence has shown that metastatic breast cancer response rates and response durations progressively decrease with increasing chemotherapy treatment.[2] Despite the remarkable development of novel diagnostic methods and therapeutic approaches, effective treatments for metastatic breast cancer are still

Correspondence: Ni Xie
Email xn100@szu.edu.cn

submit your manuscript | www.dovepress.com
DovePress
http://doi.org/10.2147/IJN.S278724

limited.[3,4] Recently, combinatorial therapeutic approaches that integrate anticancer drugs with RNA interference (RNAi) have drawn increasing attention for metastatic breast cancer therapy,[5] and have posed significant challenges that need to be overcome in clinical practice. In clinical settings, combination chemotherapy, or the grouping of different therapeutic entities to exploit additive or synergistic effects, is commonly employed. This combination strategy should not only enhance therapeutic efficiency but also treat metastatic breast cancer using mechanistically different approaches, thereby enhancing therapeutic efficiency.[6–9]

Doxorubicin (Dox) is a chemotherapy drug that is commonly used to treat both early-stage and metastatic breast cancer. Similarly, small interfering RNAs (siRNAs) have been widely explored for use in combination therapy over the last few decades.[10] Recent studies have suggested that the expression level of TIE2, a tyrosine kinase receptor for angiopoietin-1 and -2, is associated with the metastasis of breast cancer.[11–13] We previously reported that inhibiting TIE2 significantly reduces Dox-resistant breast cancer metastases.[14] Hence, the co-delivery of Dox and siTIE2, an siRNA that targets TIE2 and inhibits its function, may provide an effective approach for the treatment of metastatic breast cancer by inhibiting the growth of tumours and reducing metastasis.

Owing to the low cytotoxicity and high drug-loading ability of mesoporous silica nanoparticles (MSNs), they have been investigated as a nano-platform for the co-delivery of drugs and siRNA.[15–18] During the last few years, a variety of MSNs have been successfully developed for the co-delivery of anticancer drugs and siRNA.[19–23] However, some studies confronted Dox leakage, which is problematic because it decreases the delivery efficiency of the cargo.[24,25] Therefore, scientists have also focused significant attention on preventing this problem, with the most commonly used method involving coating the MSN surface to prevent Dox leakage. Inspired by a study that used Dox as a gatekeeper of the MSN delivery system,[18] we speculated that nucleic acids can also be employed to block cargo leakage. Moreover, MSN surfaces are readily functionalised with various molecules that can encapsulate therapeutic compounds or provide receptor recognition units.[26,27] Consequently, in this study, we explored modifying MSN surfaces with two kinds of nucleic acid, including RNA and DNA, as a coating and for the concurrent controlled release of MSNs.

Herein, we report a tumour-targeted and redox-responsive functionalised MSN nanosystem for the treatment of metastatic breast cancer. Specifically, we exploited novel Dox-loaded MSNs functionalised with disulfide bonds and with two different types of nucleic acid on their surfaces (Scheme 1): a DNA aptamer (AS1411) that serves as a cancer-targeting ligand,[28,29] and an siRNA to inhibit TIE2 (siTIE2) and induce anti-metastatic effects.[30] AS1411, which was found to have a high affinity for nucleolin, was used to improve cancer-targeting ability.[31,32] Moreover, functionalisation of the MSNs with both nucleic acids provides redox-responsive gatekeepers for the triggered release of Dox within cancer cells. Hence, functionalised MSNs can bind to the cell surface of nucleolin – a membrane protein that can migrate to the nucleus, and is overexpressed on the surface of rapidly proliferating cancer cells – for receptor-mediated drug delivery. Once the functionalised MSNs are internalised by cancer cells, high concentrations of intracellular redox molecules, such as glutathione (GSH), trigger the release of siTIE2 and Dox. We demonstrate that the functionalised MSNs efficiently inhibit the progression of metastatic breast cancer.

Materials and Methods

Materials

Tetraethyl orthosilicate (TEOS, 99%), cetyltrimethylammonium bromide (CTAB, BioXtra, ≥99%), (3-Mercaptopropyl) trimethoxysilane (MPTMS, 95%), and Pluronic® F-127 (F127, ≥99%), 4, 4′-dithiodipyridin (DTDP, 98%), dithiothreitol (DTT, ≥98%) were purchased from Sigma-Aldrich. And the other chemicals were purchased from Aladdin Chemical manufacturers (shanghai). The recombinant human nucleolin protein was purchased from Abcam. Doxorubicin hydrochloride (Dox) was purchased from Merck. The sequence of TIE2 siRNA was as following, 5′- CCAGGUAUAUAG GAGGAAATTUUUCCUCCUAUAUACCUGGTT-3′. The sequence of Aptamer AS1411 was as following, 5′-GGTGGTGGTGGTTGTGGTGGTGGTGGTT-3′. All the thiol oligonucleotides were synthesized by Shanghai GenePharma Co., Ltd. (Shanghai, China).

Cell Culture

MDA-MB-231 and HEK293T cell lines were obtained from the American Type Culture Collection (ATCC; Manassas, VA). These cells were grown in DMEM (Gibico), which was supplemented with 10% (vol/vol)

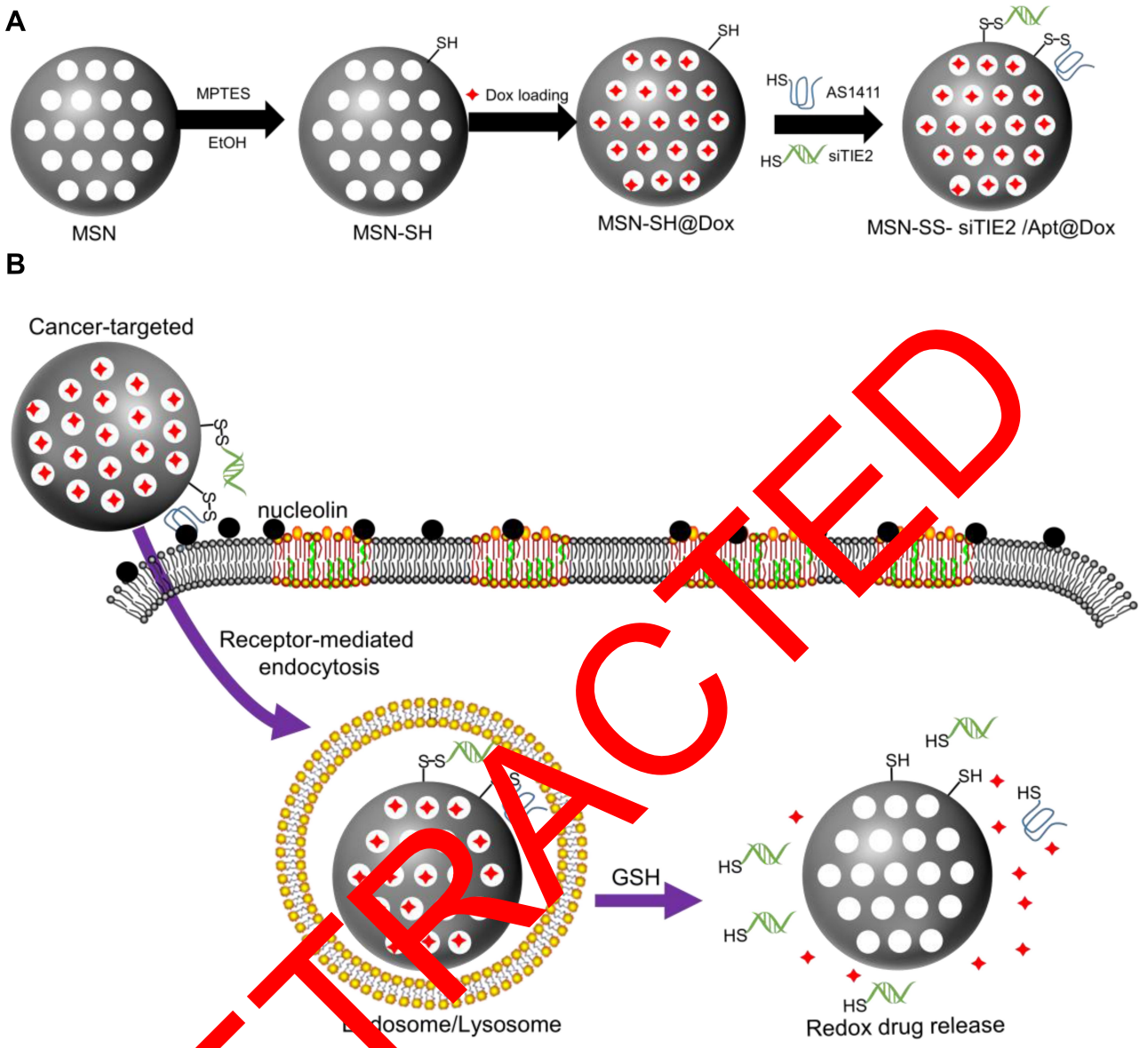

Scheme 1 Schematic representation of aptamer-based cancer-targeted and redox-responsive MSN co-delivery Dox and siRNA. (**A**) The synthesis procedure for MSN-siRNA/Apt@Dox. (**B**) The intracellular trafficking of the nanoparticles and the release of siRNA and Dox within the cancer cells.

FBS (Gibico), 100 penicillin, streptomycin, and 2 μg/mL blasticidin at 37°C in a humidified atmosphere of 5% CO_2. Cells were harvested by treatment with 0.25% trypsin-EDTA (Gibico).

Synthesis of the Nanoparticles

The MSNs were synthesized via the method reported by Bouchoucha et al.[27] Briefly, 1.0 g of CTAB and 8 g of F127 were mixed in 85 mL of 100% EtOH and 213 mL of 2.9 wt % NH4OH solution in 500 mL conical flask. A 3.86 mL of TEOS was added slowly for 4 min by stirring at 500 rpm at room temperature. Then, the mixture was aged for 24 h under static conditions at room temperature. The surfactant was removed by methanol/HCL (500:19 v/v) at 40°C for 12 h to remove the CTAB template. Then, the product was washed three times in methanol and water sequentially and dried in vacuum at 80°C overnight. The resulting NPs are designated as MSN. Next, 1.0 mL of MPTMS was added to bare particles (100 mg dissolved in 30 mL EtOH) for the production of MSN-SH. The reaction mixture was stirred for a further 24 h at room temperature. Then, the particles were separated by centrifugation (10,000 rpm, 5 min), washed with EtOH and water sequentially and dried in vacuum at 80°C overnight. Then, the DTDP (20 mg, 50 mg/mL, in EtOH) was added to MSN-SH (10 mg, 10 mg/mL, in EtOH) and the

mixture was stirred at room temperature for 24 h. The pyridine-activated particles (MSN-Py) were collected by centrifugation and washed three times in methanol and water sequentially and dried in vacuum at 80°C overnight. Then, the 10 mg of MSNs-Py was dispersed in 1 mL of Dox solution (1 mg/mL) and stirred for 12 h at room temperature. Finally, thiol-functionalized oligonucleotides including siRNA and DNA aptamer were added into the solution to immobilized on the surface of MSN-Py@Dox to block the mesopores by a disulfide exchange reaction. The oligonucleotides were freshly activated before usage by the addition of DTT (60 μmol, 1 M), followed by subsequent purification with dextran desalting columns. The exchange reaction was carried out at room temperature for 24 h, followed by centrifugation at 10,000 rpm for 3 min and washed with water. The DNA-conjugated particles are denoted as MSN-siRNA/Apt@Dox.

Quantification of Immobilized Oligonucleotides

First, different amounts of aptamer-SH and siRNA-SH solution (0.1 mg/mL) and MSN solution (0.5 mg/mL) were mixed to obtain different weight ratios (MSN:Apt:siRNA), such as 5:1:1, 10:1:1, 15:1:1, 20:1:1 and 25:1:1. Gel retardation assay was used to determine the best binding between MSN-Py and oligonucleotides. Then, the results of agarose gel electrophoresis were obtained and the optimal reaction ratio was used to produce MSN-siRNA/Apt and the amount of unreacted oligonucleotides was quantified from the supernatant by UV/Vis (260 nm) after disulfide exchange reaction. At last, the amount of oligonucleotides conjugated on the particle surface was calculated by equation:

$$Amount\ of\ \text{oligonucleotides conjugated}\ (\%) = \frac{n_{added} - n_{\text{supernatant}}}{n_{added}} \times 100\%.$$

Where n_{added} is calculated by the amount of added oligonucleotides during disulfide exchange reaction.

Quantification of Loaded Dox

To determine the loading capacity of MSN-Py for Dox, the supernatant was collected after Dox loading and the amount of cargo remaining in the supernatant was quantified by UV/Vis (480 nm). The loading capacity of loaded Dox was calculated by equation:

$$Loading\ capacity\ (\%) = \frac{m_{added} - m_{\text{supernatant}}}{m_{added}} \times 100\%.$$

Where m_{added} is calculated by the amount of added Dox during Dox loading.

Characterization of the Nanoparticles

The morphologies of MSN and MSN-siRNA/apt were investigated by transmission electron microscope (TEM) (JEM-2100F, JEOL, Japan) at an acceleration voltage of 90 kV.

The effective hydrodynamic diameters and the zeta potentials of MSN, MSN-SH, MSN-siRNA/apt were measured by DLS using the ZetaPlus' Zeta Potential Analyzer (Brookhaven Instruments, Santa Barbara, CA, USA).

Fourier transform infrared (FT-IR) spectra of MSN, MSN-SH, MSN-siRNA/apt were recorded by Nicolet 6700 FT-IR Spectrometer (ThermoFisher, USA).

The Raman spectra of MSN, MSN-SH, MSN-siRNA/apt were measured by LabRAM HRAMIS HORIBA Scientific, France).

The porosity of MSN was assessed by a nitrogen adsorption-desorption measurement. The measurement was operated at 77 K using a TriStar II 3flex (Micromeritics, USA). The pore size distribution was determined from the nitrogen adsorption isotherms through the Barrett–Joyner–Halenda method.

The amount of siRNA and aptamer on the MSN surface were evaluated as following.

First, 0.5 mg MSN-siRNA/Apt was resuspended with DEPC-treated water. After, the NPs were treated with 5 mM GSH for 6 h, the supernatant was separated by centrifugation. Then, the sample was divided into two parts and incubated with DNase I and RNase A separately for 30 min in 37°C. At last, the amount of nucleic acid adsorbed was calculated from the concentration of the nucleic acid of the supernatant, which was measured by UV–vis spectroscopy at 260 nm.

Release of the Cargos

The release profiles of Dox from the developed nanoparticles were obtained as follows. First, MSN-siRNA/apt@Dox were dispersed in PBS (pH 7.4) without or with different stimuli (20 mM GSH, and/or 1 μg Nuleolin protein). Subsequently, the mixture was incubated at 37°C and defined aliquots of the mixture (150 μL) were removed from the reaction tube at various time points (1, 2, 3, 5, 7, 9, 10 and 24 h). The removed aliquots were centrifuged and the concentration of Dox in the supernatant was measured by UV/Vis (480 nm). The cumulative release of Dox was calculated by the equation:

$$\text{Cumulative Dox release}(\%) = \frac{c_{supperant} \times V}{m_{tested}} \times 100\%.$$

For control-release of siRNA from the developed nanoparticles was obtained as followed. First, GSH was added

to MSN-siRNA/apt (PBS, pH 7.4) to reach a final GSH concentration of 0, 0.2 and 5 mM, and incubated for 12 h. Then, the samples were electrophoresed to detect the redox-triggered release of oligonucleotides. The anti-sense RNA siTIE2 and DNA aptamer AS1411T were used as controls.

Serum Stability of siRNA in MSN-siRNA/Apt@Dox

For the assay, naked siRNA (300 ng/well siRNA), 6 mg (equivalent to 300 ng/well siRNA) MSN-siRNA/apt@Dox were incubated with 10% FBS at 37°C for 6 and 24 h. After treatment, the samples were collected and centrifuged. At last, the stability of siRNA was assessed by gel electrophoresis.

Cellular Uptake of MSN-siRNA/Apt@Dox

For the cell-selectivity study, HEK293T cells and MDA-MB-231 cells were seeded in 12-well plate before the assay. After the adherence to the plate, the cells were incubated with different Dox-loaded MSNs (1 μg Dox/well, by weight of Dox) for 8 h. After washing with PBS, the samples were fixed and stained with DAPI. The treated cell samples were observed by Olympus IX81. For each sample, the fluorescence was quantified using the mean value of n > 3 pictures.

For the flow cytometry analysis, MDA-MB-231 cells were seeded in a 6-well plate before the assay. After the adherence to the plate, the cells were incubated with different Dox-loaded MSNs (5 μg Dox/well, by weight of Dox) for 8 h. The treated cells were rinsed with PBS twice, trypsinized and fixed. The cells were re-suspended with PBS and determined by a BD FACSVerse flow cytometer (BD). The results were analyzed with Flowjo.

For the cellular accumulation study of MSN-siRNA/apt@Dox, MDA-MB-231 cells were seeded in 12-well plate before the assay. After the adherence to the plate, the cells were incubated with MSN-siRNA/apt@Dox (5 μg Dox/well, by weight of Dox) for 2, 4, 8 h. The treated cells were stained with Hoechst 33342 for 20 min, rinsed with PBS twice and observed by Olympus IX81.

Pharmacokinetic Study

Pharmacokinetic date of Dox in female BALB/c mice (n=30, per group) using free Dox, MSN@Dox and MSN-siRNA/apt@Dox, which the dose of Dox is about 1 mg/kg, via the tail vein. The treated animals were euthanized in indicated time points (at 0.166, 0.25, 0.5, 1, 2, 3, 4, 6, 8, and 24 h, after injection, 3 animals for each time point/group). Blood plasma was collected and pre-treated by protein precipitation before LC-MS/MS detection. The pharmacokinetic parameters were calculated via PKSolver.

In vivo Biodistribution Study of MSN-siRNA/Apt@Dox

A 0.1 mL of MDA-MB-231 cell suspension (1×10^7/mouse) was orthotopically inoculated in the back of female BALB/c nude mice using 50% (v/v) Matrigel. The animals were purchased from Shanghai Model Organisms Center, Inc. The experimental protocols were conducted within the Shenzhen University guidelines for animal research and were approved by the First Affiliated Hospital of Shenzhen University Institutional Animal Care and Use Committee (IACUC). Approval Number IACUC-DD-2019-07-07. Tumor volumes were monitored with a vernier caliper every three days and calculated according to the formula: tumor volume (mm3) = 0.52 × length × width2. When the tumor size reached around 200 mm3, the animals were randomly assigned into 3 groups (n=3) and administrated with free Dox, MSN@Dox and MSN-siRNA/apt@Dox, which the dose of Dox is about 1 mg/kg, via the tail vein. Then, the mice were anesthetized for imaging by the IVIS spectrum (Xenogen, USA) at 0.5 h and 8 h postinjection. After 24 h treatment, all animals were sacrificed and the organs (liver, spleen, kidney, heart, lungs, and brain) and tumors were collected for ex vivo imaging. Finally, images were analyzed using Aura Imaging Software (https://spectralinvivo.com/software/).

Cytotoxicity Analysis and in vitro Tumor Inhibition Assay

The cytotoxicity of the developed nanoparticles was determined in HEK293T cells by a Cell Counting Kit (CCK-8) assay. The cells were seeded in 96-well plates before the assay. Then, the cells were treated with an increasing level of MSN-siRNA/apt@Dox for 24 h. The cell viability was measured as a percentage relative to untreated control cells.

CCK-8 assay was conducted to study the proliferation inhibitory efficacy of different Dox formulations on MDA-MB-231 cells. The cells were seeded in 96-well plates before the assay. Then, the cells were treated with a series of different concentrations of free dox, free dox+siRNA,

MSN@Dox+siRNA and MSN-siRNA/Apt@Dox for 24 h. The cell viability was measured as a percentage relative to untreated control cells. Fifty percent cell growth inhibition (IC50) was calculated from curves constructed by plotting cell survival (%) versus dox concentration (μg/mL).

In vivo Antitumor Activity Study with MSN-siRNA/Apt@Dox

Female BALB/c nude mice were purchased from Shanghai Model Organisms Center, Inc. The experimental protocols were conducted within the Shenzhen University guidelines for animal research and were approved by the First Affiliated Hospital of Shenzhen University Institutional Animal Care and Use Committee (IACUC): Approval Number IACUC-DD-2019-07-24. The xenograft model bearing MDA-MB-231 tumors were established and randomized into four groups (n=5) when the tumors reach around 100 mm3. Then, the mice were treated with saline, free dox+ siRNA, MSN@Dox+siRNA and MSN-siRNA /Apt@Dox, which the dose of Dox is about 1 mg/kg and the dose of siRNA is about 0.5 mg/kg, every 4 days for 5 times via the tail vein. After the administration, the body weight of mice and tumor size were recorded. The organs (liver, spleen, kidney, heart, lungs, and brain) and tumor tissues of treated-mice were collected at 20 days. Then, the tumors were weighed and all samples were fixed for-malin for 24 h, followed by hematoxylin-eosin (H&E) staining.

Knock-Down of TIE2 Gene Analysis

MDA-MB-231 cells were seeded into a 6-well plate. After the adherence to the plate, the cells were treated with serum-free medium. Then, the cells were treated with PBS, naked siRNA, Lipo@siRNA (Lipofectamine2000, Invitrogen), and MSN-siRNA/apt, which the dose of siRNA is 1 μg for 24 h, and then the cells were replaced with complete culture medium. After another 36 h incubation, the cells were harvested and the protein samples were extracted for Western blot analysis. Total protein extracts were subjected to SDS-polyacrylamide gel electrophoresis (PAGE). After electrophoresis, the proteins were transferred to poly (vinylidene fluoride) (PVDF) membranes (Millipore). To block non-specific binding sites, the membranes were treated for 1 h with TBST (a mixture of Tris-buffered saline and Tween-20) containing 5% milk. Subsequently, the membranes were incubated with the primary antibody against TIE2 (ab221154, Abcam) or GAPDH (14C10, CST) for 1 h overnight at 4°C. After washing, signals were detected by HRP-conjugated secondary anti-rabbit antibody and were visualized using ProteinSimple software.

In vitro Migration Analysis

The transwell migration and wound healing assays were used to evaluate the impact of the developed nanoparticles on cell migration. For transwell migration assay, MDA-MB-231 cells were seeded in a 6-well plate and pre-treated with PBS, naked siRNA, Lipo@siRNA (Lipofectamine2000, Invitrogen) and MSN-siRNA/apt, which the dose of siRNA is 1 μg for 24 h. Then, the cells were collected, resuspended in a serum-free medium and transferred into the upper transwell chambers. The lower chamber was filled with 10% FBS-containing culture medium as the chemoattractant. After incubation for 24 h, the migrated cells in the lower chamber were fixed with 4% paraformaldehyde, stained with crystal violet for 10 min, and then observed by an optical microscope. For the quantitative assay, the crystal violet staining cells were dissolved in 33% acetic acid and their absorbance was measured at 570 nm. For wound healing assay, MDA-MB-231 cells were seeded in a 6-well plate and cultured to form a tight cell monolayer. The cells were washed with serum-free medium after the cell monolayer scratching with a -μL sterile plastic pipette tip and treated with PBS, naked siRNA, Lipo@siRNA (Lipofectamine2000, Invitrogen) and MSN-siRNA/apt, which the dose of siRNA is 1 μg for 24 h. Migrating cells at the wound front were analyzed using an inverted microscope at the indicated time.

In vivo Anti-Metastasis Study

Female BALB/c nude mice were purchased from Shanghai Model Organisms Center, Inc. The experimental protocols were conducted within the Shenzhen University guidelines for animal research and were approved by the First Affiliated Hospital of Shenzhen University Institutional Animal Care and Use Committee (IACUC): Approval Number IACUC-DD-2019-07-24. The female BALB/c nude mice were intravenously injected with 1×10^6 MDA-MB-231 cells (containing luciferase), and allowed to establish metastatic tumors primarily in lungs for 2 weeks. Then, the mice were randomly divided into four groups, and treated with saline, free dox+siRNA, MSN@Dox+siRNA and MSN-siRNA/Apt@Dox, which the dose of Dox is about 1 mg/kg and the dose of siRNA is about 0.5 mg/kg, every 3 days for 6 times via the tail

vein. The luciferase activity in each mouse was measured with an in vivo imaging system every 12 days and quantified using Aura Imaging Software (https://spectralinvivo.com/software/). Mice were killed on day 38 after the initial cell injection. The lung of the mice was collected, weighed and photographed on day 38. The number of metastatic nodules on the surface of the lungs was counted and the lungs were sliced and stained with H&E.

Results and Discussion

Synthesis and Characterisation of MSN-siRNA/Apt@Dox

To successfully construct nanocarriers for the targeted intracellular co-delivery of siRNA and drugs, we designed a strategy to encapsulate siTIE2 and Dox within MSNs and improve nanoparticle targeting ability, as illustrated in Scheme 1. MSNs were synthesised based on previous reports.[33,34] (3-Mercaptopropyl) trimethoxysilane (MPTMS), a thiol-bearing organosilane, was then introduced to the MSNs to modify their surfaces with SH groups to obtain MSN-SH. Next, Dox was loaded into the porous structure of MSN-SH through incubation prior to disulfide bond exchange. Finally, Dox-loaded MSN-SH was capped with siTIE2 and AS1411 via disulfide linkers to obtain MSN-siRNA/Apt.

The successful preparations of MSNs and MSN-siRNA/Apt were confirmed by transmission electron microscopy (TEM) (Figure 1A and B), which revealed that the MSNs are spherical in shape with an average diameter of 90–110 nm and with nucleic acid nanoshells surrounding the MSN cores. Then, we investigated the nitrogen adsorption-desorption isotherms of the nanoparticles and found that the samples exhibited typical IV features according to IUPAC nomenclature (Figure 1C), indicating the well-defined mesoporous structure. And the pore size distribution curve, which was calculated according to the Barrett–Joyner[illegible]la (BJH) method (Figure 1D), suggested that the average pore sizes of 2.9, 2.4 and 1.7 nm for MSN, MSN-SH and MSN-siRNA/Apt, respectively. The MSN-siRNA/Apt particles are larger than the unmodified MSNs as observed by dynamic light scattering (DLS), confirming the successful conjugation of siTIE2 and AS1411 (Figure 1E and Table S1). Moreover, the negatively charged siRNA and DNA aptamer conjugated with MSN also contribute to the lower zeta potential of MSN-siRNA/Apt. The Fourier-transform infrared (FT-IR) spectra of unmodified MSNs, MSN-SH, and MSN-siRNA/Apt are shown in Figure 1D. Surface functionalisation was confirmed by a decrease in the Si-OH band at 971 cm^{-1} after incubation with MPTMS. The appearance of minor peaks at approximately 2875 and 1420 cm^{-1} is attributed to C–H asymmetric

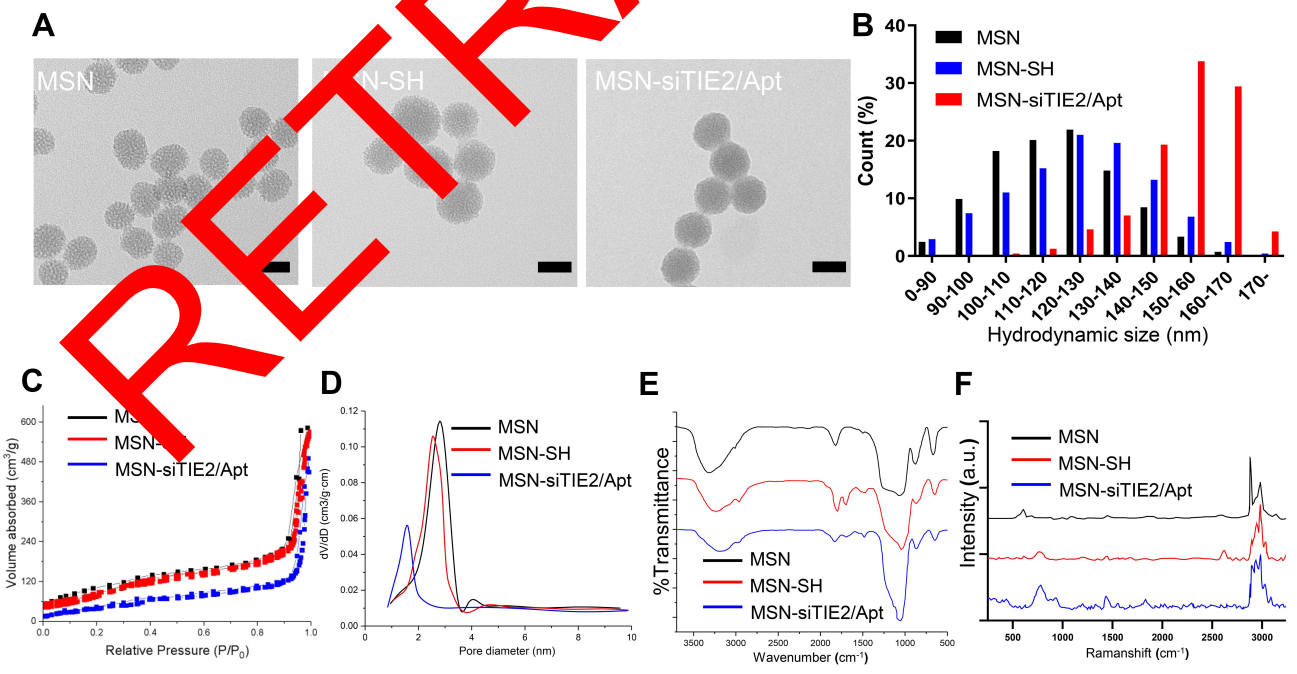

Figure 1 Characterization of MSN-siRNA/Apt. (**A**) Transmission electron microscopy (TEM) images of the MSN, MSN-SH and MSN-siRNA/Apt. (**B**) Particle size distribution of the nanoparticles. (**C**) Nitrogen adsorption-desorption isotherms of the nanoparticles. (**D**) The pore size distributions of the nanoparticles. (**E**) FTIR spectra of the nanoparticles. (**F**) Raman spectra of the nanoparticles.

stretching and rocking vibrations, respectively, in MSN-SH and MSN-siRNA/Apt, respectively. The existence of -SH groups was identified by the characteristic Raman peak at 2580 cm^{-1}, which suggests that the -SH groups from MPTMS had been grafted onto the MSN surfaces. No -SH Raman signal was detected after conjugation with thiolated SH-siTIE2 and the SH-AS1411 (Figure 1F). The successful synthesis of MSN-siRNA/Apt is supported by the abovementioned results.

The Dox loading in the prepared MSNs was determined using fluorescence spectroscopy. The MSN loading was ~8.5% at a Dox incubation concentration of 5 mg/mL. Thiolated nucleic acid binding in MSN-SH@Dox was investigated by agarose gel electrophoresis (Figure S1), which revealed that an MSN/SH-siTIE2/SH-AS1411 ratio of 20:1:1 (w/w/w) resulted in almost complete nucleic acid binding. Most of the nucleic acids were typically immobilised on the surface of MSN-siTIE2/Apt@Dox with a high conjugation efficiency (90.7%). Moreover, we also measured the amounts of siRNA and aptamer on the MSN surface, which revealed that siRNA binds more easily to the MSN surface than the aptamer at the same mass ratio to form a denser nucleic acid coating (Figure S2). In addition, the stability of siRNA on the MSN surface was evaluated; however, the results show that MSN-siRNA /Apt only moderately protected siRNA from enzyme degradation over 6 h (Figure S3).

Release of siRNA and Dox

The microenvironments of tumour cells enable redox-responsive nanocarriers to release loaded cargo in response to high levels of redox molecule[s]. Moreover, redox-responsive delivery systems are often used to increase the concentration of a drug in the cytoplasm, increase therapeutic efficacy, and reduce the toxicity of the anticancer drug. For example, redox-responsive delivery systems with disulfide bonds facilitate the release of encapsulated drug molecules within tumour cells.[36] Therefore, the cleavable disulfide linkers that attach siTIE2 and AS1411 to the MSNs should also facilitate the controlled release of Dox and siTIE2 in response to a redox trigger from MSN-siRNA /apt@Dox (Figure 2A). The functionalisation of MSNs with

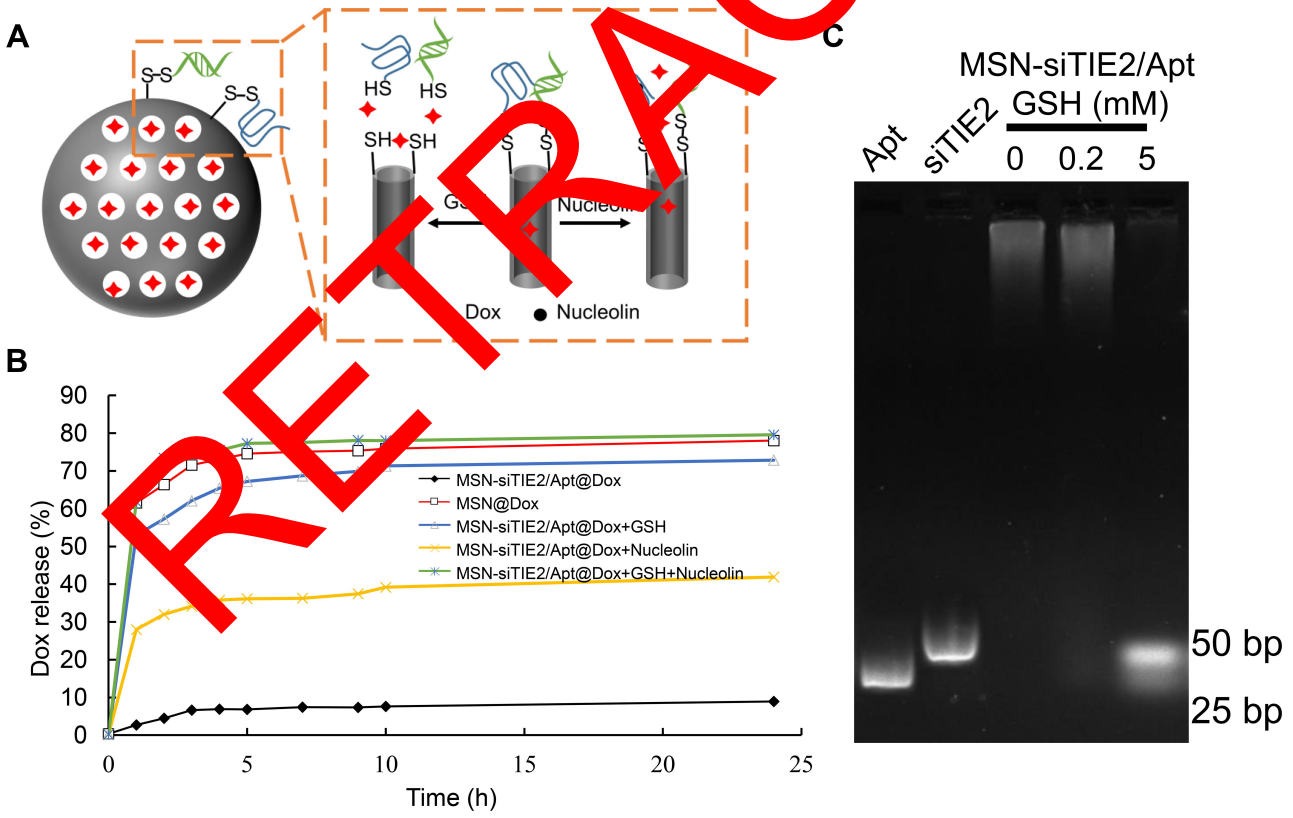

Figure 2 Nanovalve gatekeeper of MSN-siRNA/Apt@dox and the control-release profiles of DOX and siRNA. (**A**) Schematic illustration of the nuclear acid nanovalve gatekeeper installed on MSN-siRNA/apt@Dox through cleavable disulfide bonds. Cargo can be released by either redox-responsive reductive cleavage or nucleolin-induced aptamer reconfiguration. (**B**) Release profiles of DOX from the cargo-loaded nanoparticles in the presence or absence of different stimuli. (**C**) Release of siRNA from the MSN-siRNA/Apt in the increasing level of GSH.

nucleic acids was found to efficiently block the release of Dox; ie, ~71% of Dox was released from MSN-SH@Dox after 24 h in phosphate-buffered saline (PBS), whereas only 8% of Dox was released from MSN-siRNA/Apt@Dox under these conditions. Dox was released from MSN-siRNA/Apt@Dox in the presence of nucleolin or GSH. AS1411 changes its conformation through interactions with cellular nucleolin, thereby enabling the release of Dox from MSNs and acting as a "nanovalve" gatekeeper. Although both GSH and nucleolin trigger the release of Dox (Figure 2B), only small amounts of Dox were released by nucleolin, which indicates that the encapsulated Dox cannot easily be released from the AS1411 gatekeeper by interacting with nucleolin. The amount of Dox released was significantly higher (80%) in the presence of 10 mM GSH and nucleolin; therefore, most of the Dox was only released in a cellular microenvironment with a high concentration of GSH and nucleolin. In addition, we investigated the drug release behaviour of MSN-siTIE2/Apt@Dox with different GSH levels (0, 0.1, 1, 10 mM). The release profiles reveal that our developed nanoparticles exhibit GSH-concentration-dependent Dox release behaviour (Figure S4). We also did not observe any cumulative release of siTIE2 in 0.2 mM GSH (Figure 2C). In contrast, the burst release of siTIE2 was observed in response to 5 mM GSH, which indicates that only high concentrations of GSH can cleave the disulfide bonds of the attached siTIE2 to obtain efficient siTIE2 release. With this in mind, we modified the disulfide bonds on the MSN surfaces to construct an appropriate redox-responsive delivery system for the controlled release of Dox and siRNA.

Cellular Uptake Study

The targeting specificity of the developed nanoparticles was investigated using MDA-MB-231 cells (nucleolin positive) and HEK293T cells (nucleolin negative). Recent studies have used the transport mechanism of nucleolin (ie, migration from the cell surface to the nucleus) to enhance intranuclear delivery.[37,38] Therefore, we speculated that nucleolin-binding AS1411 on the MSNs will specifically direct the functionalised MSNs toward cancer cells. Confocal microscopy revealed that MSNs without AS1411 functionalisation lacked cancer cell targeting ability, and only MSN-siTIE2/Apt@Dox significantly

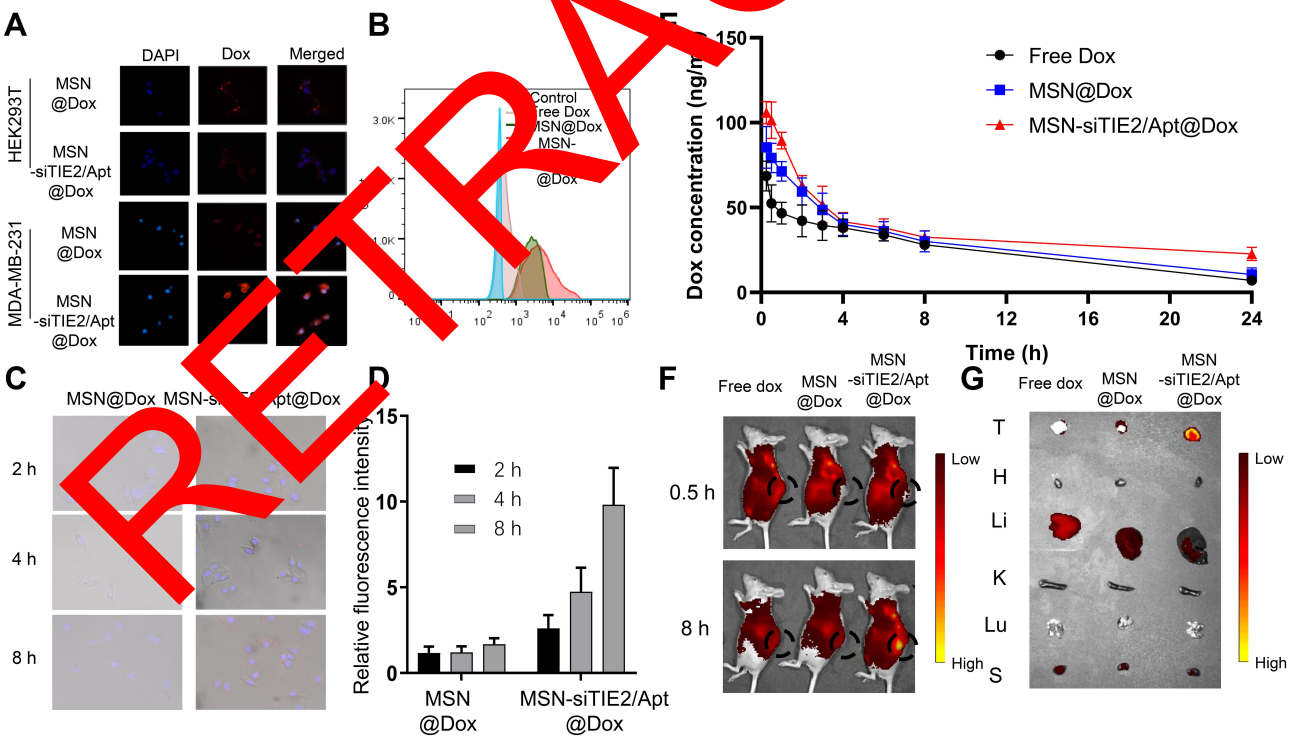

Figure 3 In vitro and In vivo evaluations of Dox delivery by developed MSN. (**A**) The cellular uptake of the nanoparticles between MDA-MB-231 cells (nucleolin positive) and HEK293T cells (nucleolin negative). (**B**) Intracellular fluorescence intensities of different Dox formulations determined by flow cytometry. (**C**) The merged images of MDA-MB-231 cells treated with MSN@Dox and MSN-siTIE2/Apt@Dox. (**D**) The cellular accumulation of Dox for MSN@Dox and MSN-siTIE2/Apt@Dox at 2, 4 and 8 h. (**E**) Plasma drug concentration (at a dose of 1 mg/kg body weight) of Free Dox, MSN@Dox and MSN-siTIE2/Apt@Dox Data show mean± SD (n=3). (**F**) In vivo fluorescent images of MDA-MB-231 tumor-bearing mice treated with different Dox-loaded nanoparticles via tail vein injection. Images were taken at 0.5 h and 8 h after injection. (**G**) The biodistribution of Dox in the organs after injection for 24 h in different groups.

increased the cellular uptake of MSNs in MDA-MB-231 cells (Figures 3A and S5). A flow cytometry assay was used to investigate the delivery of Dox in MDA-MB-231 using different Dox delivery groups (PBS, free Dox, MSN@Dox and MSN-siTIE2/Apt@Dox). Poor uptake of Dox by MDA-MB-231 cells was observed for free Dox (Figure 3B). MSN-siTIE2/Apt@Dox exhibited the strongest fluorescence in the MDA-MB-231 cells, suggesting that Dox is significantly better accumulated through incubation of the functionalised MSNs. In addition, MSN-siTIE2/Apt@Dox efficiently penetrated the MDA-MB-231 cells within 4 h and delivered Dox to the cell nuclei after treatment for 8 h (Figure 3C). Combined, these results indicate that MSN-siTIE2/Apt@Dox exhibited targeted delivery and high Dox accumulation in MDA-MB-231 cells.

Biodistribution of the MSNs in vivo

We first studied the pharmacokinetic characteristics of Dox (Figure 3D and Table S2), which revealed that Dox was rapidly released in all groups, and that the Dox level was predominantly higher in the Free Dox group. However, the concentration of Dox also decreased faster after free-Dox treatment compared with other groups. Our results demonstrate that the AUC_{0-t} values of MSN@Dox and MSN-siTIE2/Apt@Dox were higher than those of the other groups, which indicate that both MSN-based delivery systems improve Dox accumulation. Moreover, the blood circulation half-life of Dox in the MSN-siTIE2/Apt@Dox group was found to be 13.49 ± 3.68 h, which is longer than those of the free-Dox and MSN@Dox groups. Nude mice with MDA-MB-231 tumour xenografts were used to evaluate the in vivo biodistributions of free-Dox and Dox-loaded MSN formulations. A significant difference in the Dox biodistribution was observed among the various delivery groups after intravenous administration (Figure 3E). A much higher fluorescence intensity of Dox was observed at primary tumour sites from MSN-siTIE2/Apt@Dox than from MSN-SH@Dox and free Dox after circulation in the bodies of mice for 8 h (Figure 3F). The mice were euthanized after 24 h, and the major organs (ie, heart, liver, spleen, lungs, and kidneys) and tumours were collected and fluorescence imaged to quantitatively analyse the accumulation of Dox among the different groups. MSN-siRNA/Apt@Dox was revealed to be accumulated in tumours to a significantly greater extent than the other two groups (Figure 3G), which demonstrates the high tumour-targeting ability of our functionalised MSNs that enhance binding to cancer cells and increase Dox accumulation in the tumours. Notably, quantitative analysis of the fluorescence intensity of Dox present in the major organs revealed that MSN-siRNA/Apt@Dox led to less Dox accumulation in the liver and kidneys than either free Dox or MSN-SH@Dox, both of which accumulated in the liver in abundance (Figure S6). MSN-siRNA/Apt@Dox enhanced

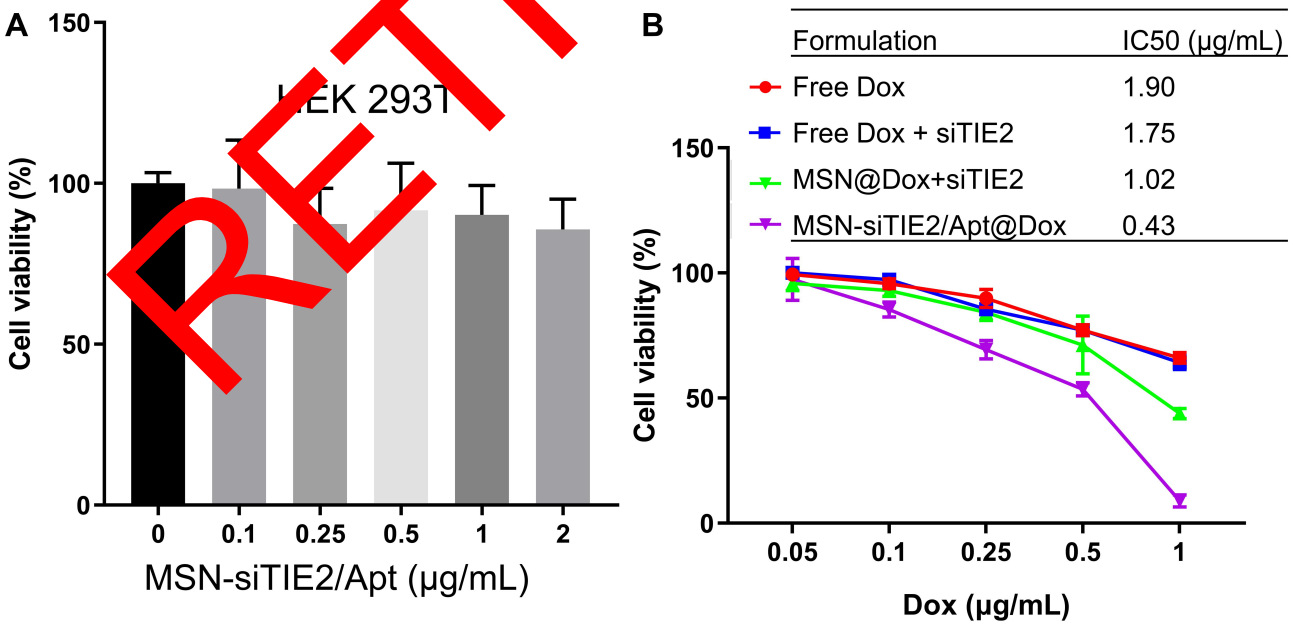

Figure 4 Cytotoxicity and the in vitro tumor inhibition effect of the developed nanoparticles. (**A**) The cytotoxicity of MSN-Apt/siRNA determined in HEK293T cells. (**B**) The viability of MDA-MB-231 cells treated with different Dox formulations.

tumour permeability and redox-responsive release of Dox in tumours instead of vital organs.

In vitro Cytotoxicity Investigation

The viabilities of HEK293T cells treated with different concentrations of unmodified MSNs were investigated using the MTT assay, which revealed that MSN-siTIE2/Apt displays little cytotoxicity against the normal cell line (Figure 4A). The IC_{50} values of free Dox and Dox-loaded MSNs were evaluated in MDA-MB-231 to determine the proliferation inhibition of tumour cells in vitro. Treatment with different Dox formulations at various concentrations for 48 h significantly affected the growth of MDA-MB-231 cells (IC50 of free Dox=1.901 μg/mL, IC50 of free Dox/free siTIE2 = 1.750 μg/mL; Figure 4B). Compared with free Dox and free Dox/free siTIE2, MSN-siTIE2/Apt@Dox exhibited enhanced antiproliferative activity, which may contribute to the larger accumulation of Dox in MDA-MB-231 cells by the MSNs. Furthermore, MSN-siTIE2/Apt@Dox exhibited increased cytotoxicity compared to the other Dox formulations investigated, as illustrated by the IC_{50} value of 0.433 μg/mL. A superior therapeutic effect on MDA-MB-231 cells was obtained from the MSN-siTIE2/Apt@Dox nano-drug delivery system.

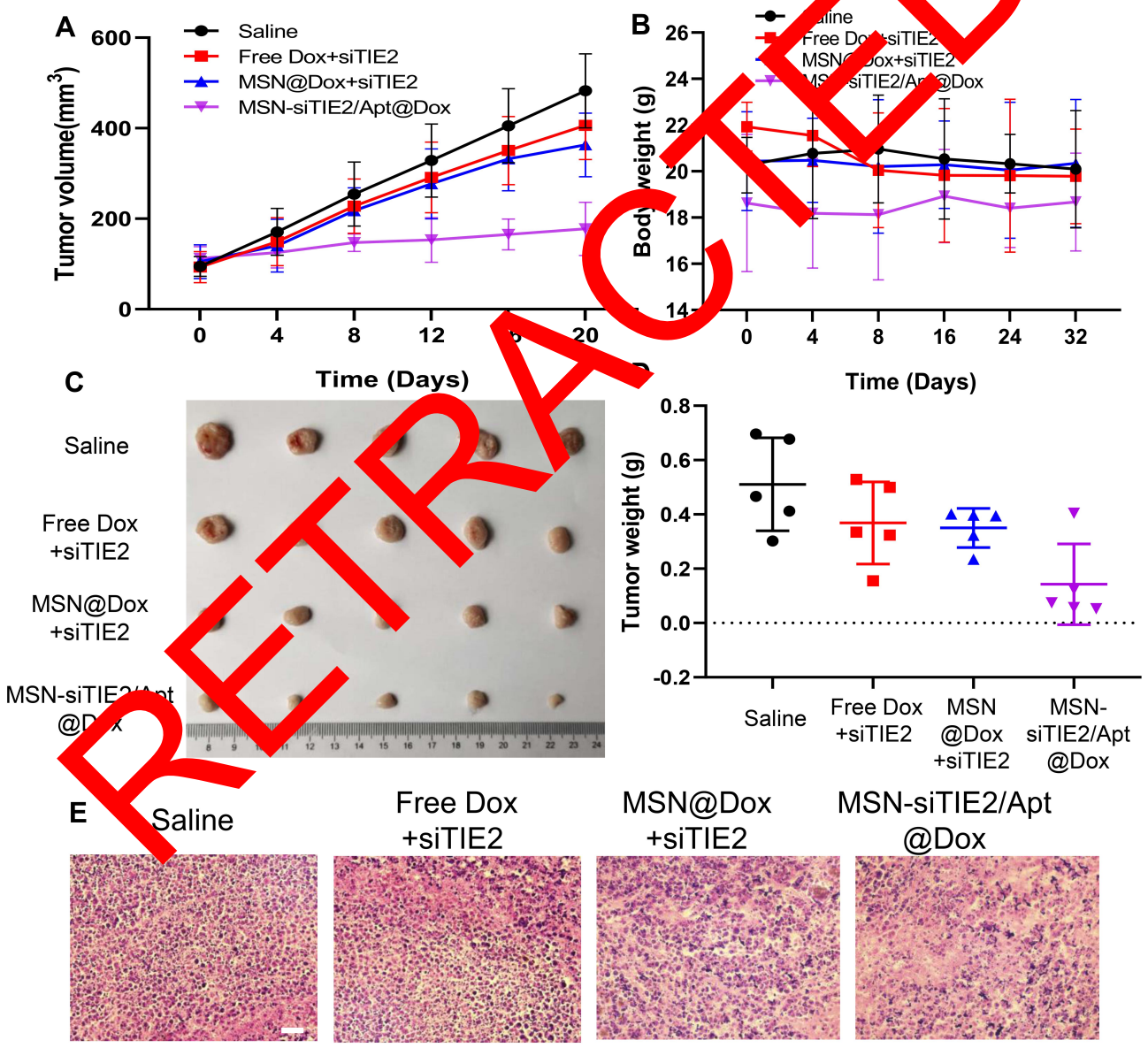

Figure 5 In vivo anti-tumor activity of different dox and siRNA-loaded nanoparticles on MDA-MB-231 tumor-bearing mice. (**A**) The tumor growth of the mice tested by different treatments. (**B**) The body weight of the mice tested by different treatments. (**C**) The images of solid tumors from the mice in each group after 20 days of treatment. (**D**) The tumor weight of the mice in different groups. (**E**) The H&E staining of the tumor in different groups.

In vivo Antitumour Efficacy

An MDA-MB-231 tumour-bearing mouse xenograft model was established to confirm the in vivo antitumour efficacies of the co-delivery systems. Because MDA-MB-231 cells are not sensitive to Dox treatment, free Dox/free siRNA did not suppress tumour growth when compared with the saline group (Figure 5A), and MSN@Dox+siTIE2 exhibited similar tumour inhibition to that of free Dox/free siTIE2. However, remarkable inhibition of tumour growth was observed with MSN-siTIE2/Apt@Dox. Furthermore, injection of MSN-siTIE2/Apt@Dox did not affect the body weights of the mice, whereas free Dox/free siTIE2 led to lower body weights during the early stages of treatment (Figure 5B), indicating that the functionalized MSNs are not systemically toxic. At the end of the animal study, the tumours were removed from the mice and weighed to further investigate tumour inhibition. MSN-siTIE2/Apt@Dox displayed the best tumour growth inhibition compared to the other groups (Figure 5C and D). Sections of the major organs and tumours were analysed by H&E staining; no obvious morphological damage to the major organs in most of the groups was observed, with only a minor change in the liver observed in the free Dox+siTIE2 group, suggesting that the functionalised MSNs improve the biocompatibility of free Dox (Figure S7). MSN-siTIE2/Apt@Dox presented large necrotic regions in tumour when compared with the other groups (Figure 5E). Considering these findings, MSN-siTIE2/Apt@Dox is promising for tumour inhibition against MDA-MB-231 cells and the suppression of breast cancer metastasis.

In vitro Cell Migration and Invasion Experiments

Since inhibition of TIE2 was found to result in inhibition of cancer cell migration and tumour invasion in our previous findings,[39,40] the anti-metastatic effect of MSN-siRNA/Apt was assessed in vitro. Notably, Dox was found to impact cell migration and invasion in previous studies;[41,42] consequently, Dox was not loaded into the siRNA formulations in our in vitro anti-metastasis study. First, the TIE2 protein expression among different treatments was investigated to determine the knockdown effect of siTIE2. The negative control, naked siTIE2, did not impact the expression of TIE2, while positive siTIE2 transfection with Lipo 2000 effectively inhibited expression (Figure 6A). Furthermore, the expression of TIE2 was dramatically reduced by MSN-siRNA/Apt@Dox, which confirmed that the functionalised MSNs knockdown TIE2 expression. We found that the number of invading cells was sharply lower after MSN-siRNA/Apt treatment (Figure 6B and C). Furthermore, the migration capacity of MDA-MB-231 cells was significantly suppressed by Lipo@siTIE2 (liposomes carrying siTIE2) and MSN-siRNA/Apt (Figure 6D and E). Consequently, our functionalized MSNs exhibited both lower cell invasion and migration.

In vivo Anti-Metastatic Effect

A pulmonary metastasis model was established to evaluate the anti-metastasis outcome of MSN-siRNA/Apt@Dox. After the initial intravenous injection of MDA-MB-231-Luc cells in mice, Dox was administered with different Dox formulations every three days from day 14 onwards. In vivo bioluminescence imaging was then employed to monitor metastasis of each Dox formulation on days 14, 26, and 38 after cell injection. We found that the intensities of the bioluminescence signals of MSN@Dox+siTIE2 slightly decreased during tumour metastasis in mice (Figure 7A and B); however, its anti-metastatic ability was similar to that of the free Dox+siTIE2 treatment. The difference in biodistribution between MSN-SH and MSN-siTIE2/Apt might contribute to the difference in anti-metastatic ability. Accordingly, since MSN-siTIE2/Apt@Dox accumulated more in tumours, the functionalised MSNs exhibited a remarkable reduction in tumour metastasis. Metastatic nodules in the lungs were also identified to characterise the anti-metastatic ability of MSN-siRNA/Apt@Dox (Figures 7C and S8). Metastatic nodules were obvious in the saline and free Dox+siRNA groups, while MSN-siRNA/Apt@Dox displayed a lower degree of tumour metastasis. H&E staining further verified the anti-metastatic ability of MSN-siRNA/Apt@Dox, with fewer metastatic foci present in the lungs (Figure 7D). The functionalised MSNs clearly suppressed the pulmonary metastasis of MDA-MB-231.

Conclusion

We demonstrated that our functionalised MSNs are effective as a nanomedicine with both chemotherapeutic and

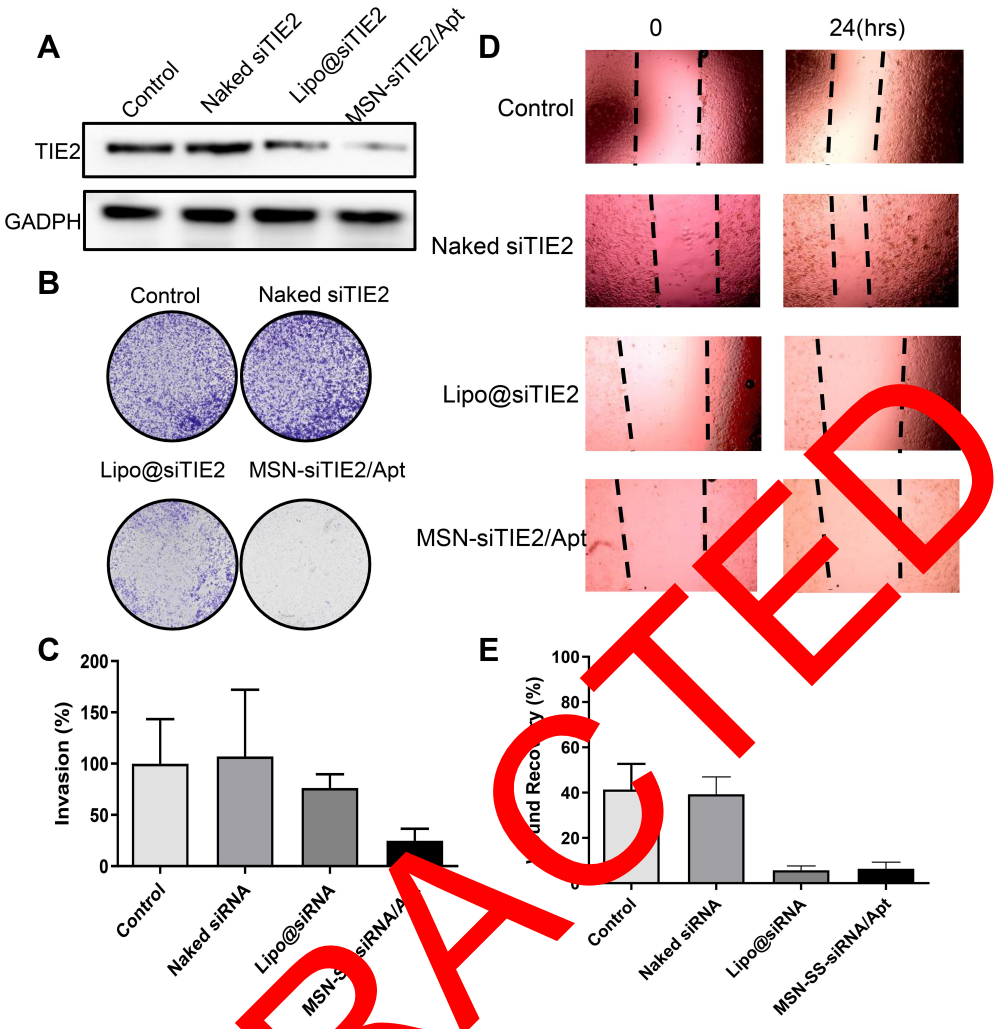

Figure 6 Anti-metastasis effect of MSN-siRNA/[illegible] in vitro. (**A**) The protein expression of TIE2 in MDA-MB-231 cells with different treatments. (**B**) The images of invasion of MDA-MB-231 cells after different treatments. (**C**) Quantitative cell invasion in different groups. (**D**) The images of migration of MDA-MB-231 cells after different treatments. (**E**) Quantitative cell migration in different groups.

gene therapeutic actions against metastatic breast cancer, thereby providing tumour-targeted delivery and redox-responsive release. In our design, the tumour-targeted delivery of functionalized MSNs selectively transported Dox to specific cells, which greatly enhanced the therapeutic efficacy of Dox against MDA-MB-231 cells. Furthermore, the DNA aptamer AS1411 and the siRNA (siTIE2) nucleic acids attached to the surfaces of the MSNs through disulfide bonds act as gatekeepers that prohibit the leakage of Dox into circulation and prevent the degradation of siTIE2 molecules. Our co-delivery system was, therefore, able to inhibit the growth of MDA-MB-231 cells and downregulate TIE2 expression, and exhibited outstanding synergism for treatment of metastatic breast cancer. The functionalized MSNs presented in this study provide a promising strategy that combines chemotherapy with gene therapy for the treatment of metastatic breast cancer, a type of cancer that is difficult to treat clinically and which benefits from multi-mechanistic treatment methods.

Acknowledgments

This work was supported by the Natural Science Foundation of National (81902672, 81972003), the Natural Science Foundation of Guangdong (2016A030313029, 2017A030313668), Sanming Project of Medicine in Shenzhen

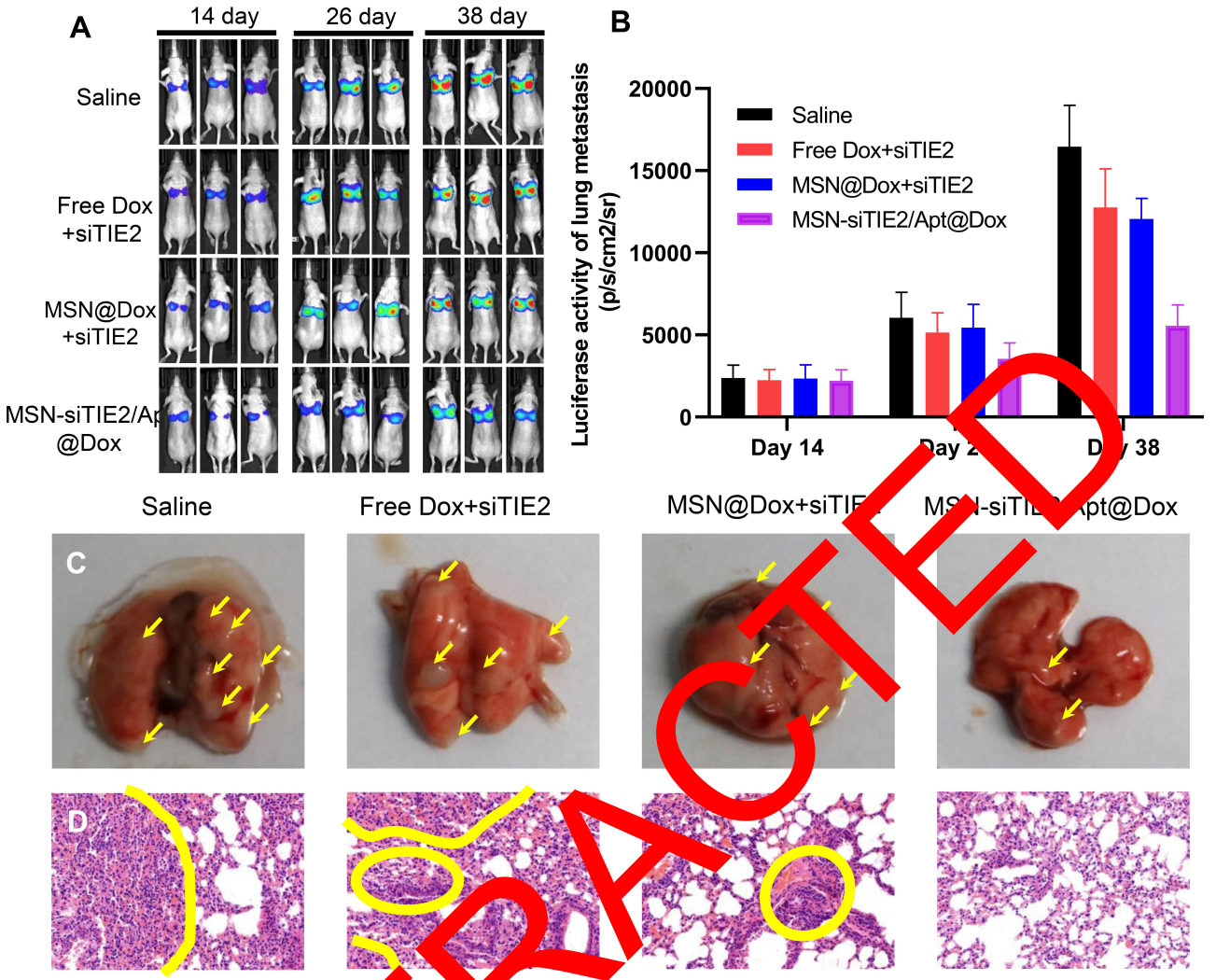

Figure 7 Anti-metastasis effect of MSN-siRNA/A vivo. (**A**) The b minescent images of the pulmonary metastasis models after tail vein injection of MDA-MB-231 cells in different groups at day 14, 26, and 38. (**B**) T qua tive biolumine t intensity in different groups. (**C**) The images of lung collected from the pulmonary metastasis models treated with different formulations, the yellow ar s indicate the metastatic nodules. (**D**) Typical histopathologic examination of lungs in different groups, the areas within the yellow circles are the area c ell necrosis, indic the presence of tumor cell infiltration.

(SZSM201612031), Sh nzhen Municipal Government of China (JCYJ20170817 08368, CYJ201708180856 57917, JCYJ20 050 8464 04, J QTD201708101602260 82), the m jor scie tific and technological project of Guangdong Province (No.2017B030308006, 2020A15151104) and the major program for tackling key problems of Guangzh City, China (No. 201704020144).

Disclosure

The authors declare no competing interests.

References

1. Waks AG, Winer EP. Breast cancer treatment: a review. *JAMA*. 2019;321(3):288–300. doi:10.1001/jama.2018.19323
2. Sledge GW. Curing metastatic breast cancer. *J Oncol Pract*. 2016;12(1):6–10. doi:10.1200/JOP.2015.008953
3. Wormann B. Breast cancer: basics, screening, diagnostics and treatment. *Med Monatsschr Pharm*. 2017;40(2):55–64.
4. Sambi M, Qorri B, Harless W, Szewczuk MR. Therapeutic options for metastatic breast cancer. *Adv Exp Med Biol*. 2019;1152:131–172.
5. Esteva FJ, Hubbard-Lucey VM, Tang J, Pusztai L. Immunotherapy and targeted therapy combinations in metastatic breast cancer. *Lancet Oncol*. 2019;20(3):e175–e186. doi:10.1016/S1470-2045(19)30026-9
6. Brandao M, Ponde NF, Poggio F, et al. Combination therapies for the treatment of HER2-positive breast cancer: current and future prospects. *Expert Rev Anticancer Ther*. 2018;18(7):629–649. doi:10.1080/14737140.2018.1477596
7. Escriva-de-Romani S, Arumi M, Bellet M, Saura C. HER2-positive breast cancer: current and new therapeutic strategies. *Breast*. 2018;39:80–88. doi:10.1016/j.breast.2018.03.006
8. Li Y, Li X, Lu Y, et al. Co-delivery of poria cocos extract and doxorubicin as an 'all-in-one' nanocarrier to combat breast cancer multidrug resistance during chemotherapy. *Nanomedicine*. 2020;23:102095. doi:10.1016/j.nano.2019.102095

9. Zhou Z, Kennell C, Lee JY, Leung YK, Tarapore P. Calcium phosphate-polymer hybrid nanoparticles for enhanced triple negative breast cancer treatment via co-delivery of paclitaxel and miR-221/222 inhibitors. *Nanomedicine*. 2017;13(2):403–410. doi:10.1016/j.nano.2016.07.016
10. Kaur K, Rath G, Chandra S, Singh R, Goyal AK. Chemotherapy with si-RNA and anti-cancer drugs. *Curr Drug Deliv*. 2018;15(3):300–311. doi:10.2174/1567201814666170518141440
11. Kitajima D, Kasamatsu A, Nakashima D, et al. Tie2 regulates tumor metastasis of oral squamous cell carcinomas. *J Cancer*. 2016;7(5):600–607. doi:10.7150/jca.13820
12. Jayson GC, Zhou C, Backen A, et al. Plasma Tie2 is a tumor vascular response biomarker for VEGF inhibitors in metastatic colorectal cancer. *Nat Commun*. 2018;9(1):4672. doi:10.1038/s41467-018-07174-1
13. Teichert M, Milde L, Holm A, et al. Pericyte-expressed Tie2 controls angiogenesis and vessel maturation. *Nat Commun*. 2017;8(1):16106. doi:10.1038/ncomms16106
14. Tang X, Shi L, Xie N, et al. SIRT7 antagonizes TGF-beta signaling and inhibits breast cancer metastasis. *Nat Commun*. 2017;8(1):318. doi:10.1038/s41467-017-00396-9
15. Chen W, Glackin CA, Horwitz MA, Zink JI. Nanomachines and other caps on mesoporous silica nanoparticles for drug delivery. *Acc Chem Res*. 2019;52(6):1531–1542. doi:10.1021/acs.accounts.9b00116
16. Hai L, Jia X, He D, et al. DNA-functionalized hollow mesoporous silica nanoparticles with dual cargo loading for near-infrared-responsive synergistic chemo-photothermal treatment of cancer cells. *ACS Appl Nano Mater*. 2018;1(7):3486–3497. doi:10.1021/acsanm.8b00657
17. Zhao S, Xu M, Cao C, Yu Q, Zhou Y, Liu J. A redox-responsive strategy using mesoporous silica nanoparticles for co-delivery of siRNA and doxorubicin. *J Mater Chem B*. 2017;5(33):690[illegible]69[illegible] doi:10.1039/C7TB00613F
18. Cheng W, Liang C, Wang X, et al. A drug-self-gated and [illegible]-microenvironment-responsive mesoporous silica [illegible]: "four-in-one" versatile nanomedicine for targeted multidrug-resistant cancer therapy. *Nanoscale*. 2017;9(43):1706[illegible]17073. [illegible]:10.1039/C7NR05450E
19. Liu CM, Chen GB, Chen HH, et al. [illegible]cancer cell membrane-cloaked mesoporous silica nanoparticles with a pH-sensitive gatekeeper for cancer treatment. *Colloids Surf B Biointerfaces*. 2019;[illegible]5:477–486. doi:10.1016/j.colsurfb.2018.12.038
20. Shen Y, Li M, Li T, et al. A [illegible]al-functional HER2 aptamer-conjugated pH-activated mesoporous silica nanocarrier-based drug delivery system provides in vitro synergistic cytotoxicity [illegible]ER2-positive breast cancer cells. *Int J [illegible]dicine*. 2019;14:4029–4044. doi:10.2147/IJN.S216[illegible]
21. Pasc[illegible]L, Cerqueira-Coutinho C, Garcia-Fernandez A, et al. MUC1 aptamer-[illegible]capped mesoporous silica nanoparticles for controlled drug delivery and radio-imaging applications. *Nanomedicine*. 2017;13(8):2495–25[illegible]doi:10.1016/j.nano.2017.08.006
22. Lio DCS, Liu [illegible]Oo MMS, et al. Transdermal delivery of small interfering RNAs with topically applied mesoporous silica nanoparticles for facile skin cancer treatment. *Nanoscale*. 2019;11(36):17041–17051. doi:10.1039/C9NR06303J
23. Sun P, Leidner A, Weigel S, et al. Biopebble containers: DNA-directed surface assembly of mesoporous silica nanoparticles for cell studies. *Small*. 2019;15(20):e1900083. doi:10.1002/smll.201900083
24. Bahadorikhalili S, Ma'mani L, Mahdavi H, Shafiee A. Copper supported β-cyclodextrin functionalized PEGylated mesoporous silica nanoparticle -graphene oxide hybrid: an efficient and recyclable nano-catalyst for straightforward synthesis of 2-arylbenzimidazoles and 1,2,3-triazoles. *Microporous Mesoporous Mater*. 2018;262:207–216. doi:10.1016/j.micromeso.2017.11.046
25. Hartono SB, Hadisoewignyo L, Yang Y, Meka AK, Antaresti A, Yu C. Amine functionalized cubic mesoporous silica nanoparticles as an oral delivery system for curcumin bioavailability enhancement. *Nanotechnology*. 2016;27(50):505605. doi:10.1088/0957-4484/27/50/505605
26. Li T, Shen X, Geng Y, et al. Folate-functionalized magnetic-mesoporous silica nanoparticles for drug/gene codelivery to potentiate the antitumor efficacy. *ACS Appl Mater Interfaces*. 2016;8(22):13748–13758. doi:10.1021/acsami.6b02963
27. Bouchoucha M, Cote MF, C.-Gaudreault R, Fortin MA, Kleitz F. Size-Controlled Functionalized Mesoporous Silica Nanoparticles for Tunable Drug Release and Enhanced Anti-Tumoral Activity. *Chem Mater*. 2016;28(12):4243–4258.
28. Li X, Wu X, Yang H, [illegible]L, Ye[illegible] Rao Y. [illegible]nuclear targeted Dox-aptamer loaded liposome delivery platform for the circumvention of drug resistance in breast cancer. *Biomed Pharmacother*. 2019;117:109072. doi:10.1016/j.biopha.2019.109072
29. Sacko K, Th[illegible]gavel [illegible]hoyele SA. Codelivery of genistein and miRNA-29[illegible] to A549 cells using aptamer-hybrid nanoparticle bioconjugate. *Nanomaterials (Basel)*. 2019;9(7):1052. doi:10.3390/nano9071052
30. Harney AS, Karagiannis GS, Pignatelli J, et al. The selective Tie2 inhibitor rebastinib blocks recruitment and function of Tie2(Hi) macrophages in breast cancer and pancreatic neuroendocrine tumors. *Mol Cancer Ther*. 2017;16(11):2486–2501. doi:10.1158/1535-7163.MCT-17-0241
31. Hernandez J, Hernandez LI, Pinto A, Schafer T, Ozalp VC. Targeting cancer cells with controlled release nanocapsules based on a single aptamer. *Chem Commun (Camb)*. 2013;49[illegible]:1285–1287. doi:10.1039/c2cc37370j
32. Sun H, Zu Y. Aptamers and their applications in nanomedicine. *Small*. 2015;11(20):2352–2364. doi:10.1002/smll.201403073
33. Zhuang J, Zhang J, Wu M, Zhang Y. A dynamic 3D tumor spheroid chip enables more accurate nanomedicine uptake evaluation. *Adv Sci (Weinh)*. 2019;6(22):1901462. doi:10.1002/advs.201901462
34. Bouchoucha M, Côté M-F, C.-Gaudreault R, Fortin M-A, Kleitz F. Size-controlled functionalized mesoporous silica nanoparticles for tunable drug release and enhanced anti-tumoral activity. *Chem Mater*. 2016;28(12):4243–4258. doi:10.1021/acs.chemmater.6b00877
35. Gao Y, Jia L, Wang Q, et al. pH/Redox dual-responsive polyplex with effective endosomal escape for codelivery of siRNA and doxorubicin against drug-resistant cancer cells. *ACS Appl Mater Interfaces*. 2019;11(18):16296–16310. doi:10.1021/acsami.9b02016
36. Chen X, Zhang Y, Tang C, et al. Co-delivery of paclitaxel and anti-survivin siRNA via redox-sensitive oligopeptide liposomes for the synergistic treatment of breast cancer and metastasis. *Int J Pharm*. 2017;529(1–2):102–115. doi:10.1016/j.ijpharm.2017.06.071
37. Yang S, Ren Z, Chen M, et al. Nucleolin-targeting AS1411-aptamer-modified graft polymeric micelle with dual ph/redox sensitivity designed to enhance tumor therapy through the codelivery of doxorubicin/TLR4 siRNA and suppression of invasion. *Mol Pharm*. 2018;15(1):314–325. doi:10.1021/acs.molpharmaceut.7b01093
38. Mosafer J, Mokhtarzadeh A. Cell surface nucleolin as a promising receptor for effective AS1411 aptamer-mediated targeted drug delivery into cancer cells. *Curr Drug Deliv*. 2018;15(9):1323–1329. doi:10.2174/1567201815666180724104451

39. Li P, Wang J, Wu D, et al. ERRα is an aggressive factor in lung adenocarcinoma indicating poor prognostic outcomes. *Cancer Manag Res*. 2019;11:8111–8123. doi:10.2147/CMAR.S204732
40. Yang F, Chen S, He S, Huo Q, Hu Y, Xie N. YB-1 interplays with ERalpha to regulate the stemness and differentiation of ER-positive breast cancer stem cells. *Theranostics*. 2020;10(8):3816–3832. doi:10.7150/thno.41014
41. Liu CL, Chen MJ, Lin JC, et al. Doxorubicin promotes migration and invasion of breast cancer cells through the upregulation of the RhoA/MLC pathway. *J Breast Cancer*. 2019;22(2):185–195. doi:10.4048/jbc.2019.22.e22
42. Huo Q, Li Z, Cheng L, Yang F, Xie N. SIRT7 is a prognostic biomarker associated with immune infiltration in luminal breast cancer. *Front Oncol*. 2020;10:621. doi:10.3389/fonc.2020.00621